CHROMATIN BIOPHYSICS

Stochastic motion and transcriptional dynamics of pairs of distal DNA loci on a compacted chromosome

David B. Brückner¹†, Hongtao Chen^{2,3}†, Lev Barinov^{3,4}, Benjamin Zoller^{5,6}, Thomas Gregor^{3,5,6}*

Chromosomes in the eukaryotic nucleus are highly compacted. However, for many functional processes, including transcription initiation, the pairwise motion of distal chromosomal elements such as enhancers and promoters is essential and necessitates dynamic fluidity. Here, we used a live-imaging assay to simultaneously measure the positions of pairs of enhancers and promoters and their transcriptional output while systematically varying the genomic separation between these two DNA loci. Our analysis reveals the coexistence of a compact globular organization and fast subdiffusive dynamics. These combined features cause an anomalous scaling of polymer relaxation times with genomic separation leading to long-ranged correlations. Thus, encounter times of DNA loci are much less dependent on genomic distance than predicted by existing polymer models, with potential consequences for eukaryotic gene expression.

iving systems are built based on information encoded in chromosomes confined in each cell's nucleus. These meter-long DNA polymers must be highly compacted to fit into the micrometer-sized structure (1, 2). At the same time, for cells to function, chromosome organization must allow the information content to be accessed and read out through transcription (3, 4). Often, transcription can only occur through the spatial interaction of DNA loci such as enhancers and promoters, which find each other dynamically and remain in physical proximity (5-8). Although the distances over which many enhancers function in higher eukaryotes can be up to mega-base pairs in genomic separation (9-12), it is unknown how these elements come into proximity, what their typical distance is in three-dimensional (3D) space, and how they explore this space dynamically in the process. Specifically, it remains unclear how the real-time physical motion of such coupled pairs of DNA loci determines transcriptional encounters and how this depends on their genomic separation.

Over the past decade, the advent of chromosome capture and imaging methods (13) has given key insights into the 3D spatial organization of chromosomes, with the discovery of structural features such as topologically associating domains (TADs) (14–17), phase-separated nuclear condensates (18–20), and larger-scale compartments (21, 22). These or-

Institute of Science and Technology, Am Campus 1, Klosterneuburg, Austria. ²School of Life Science and Technology, ShanghaiTech University, Shanghai, China. ³Lewis-Sigler Institute for Integrative Genomics, Princeton University, Princeton, NJ, USA. ⁴Memorial Sloan Kettering Cancer Center, New York, NY, USA. ⁵Joseph Henry Laboratories of Physics, Princeton University, Princeton, NJ, USA. ⁶Department of Developmental and Stem Cell Biology, CNRS UMR3738 Paris Cité, Institut Pasteur, Paris, France.

*Corresponding author. Email: tg2@princeton.edu †These authors contributed equally to this work.

ganizing structures have key implications for transcriptional regulation (23), but they are not static. Rather, they have been revealed to be heterogeneous across cells (24, 25) and dynamic and short lived in time (26, 27). The role of the real-time dynamics of pairs of loci is only beginning to be understood and remains elusive for focal contacts that are key to establishing enhancer-promoter interactions in many systems (28).

Similarly, from a polymer physics perspective, there is a gap in our understanding of the static and dynamic properties of chromosomes. At large scales, across tens to hundreds of TADs, chromosome organization has been shown to be highly compacted in a space-filling configuration (22, 29, 30). A useful null model for this configuration is the crumpled chain (also referred to as fractal globule) with fractal dimension three (22, 31-33). However, the real-time dynamics of DNA loci revealed by live-imaging experiments exhibit subdiffusion with exponents in the range of 0.5 to 0.6 (26, 27, 34-36), close to the predictions of the simple Rouse polymer model, which predicts a loosely packed ideal chain polymer configuration with fractal dimension two that is in contrast to the compacted architecture of the crumpled chain model. A promising technique to address this gap are scaling approaches that combine fractal organization and subdiffusive dynamics (37-39), but these have never been tested experimentally.

Thus far, experimental datasets have given insight into static organization (14–17, 22, 30, 40), dynamic properties of chromosomes (26, 27, 34, 35, 41), or transcription (8, 36, 42–44), but rarely all at the same time. For instance, previous live measurements of locus pairs occurred at fixed genomic separation in transcriptionally silent loci (26, 27). To investigate how 3D spatial organization and dynamic locus motion control the encounter times of functional DNA loci and thus transcriptional activation,

we require an approach to simultaneo monitor the movement of DNA locus pand transcription across a series of genomic separations in vivo.

Here, we addressed this problem by live imaging the joint dynamics of two cis-regulatory DNA elements, an enhancer and a promoter, while monitoring the transcriptional output resulting from their functional dynamic encounters in developing fly embryos. We systematically varied the genomic separation between these loci spanning many TADs. Stochastic real-time trajectories of the 3D motion of the two loci showed a dynamic search process, with physical proximity required for successful transcription and a power-law scaling of transcription probability with genomic separation. Although typical 3D distances between the locus pair follow a compact packing consistent with the crumpled chain model, the dynamic properties exhibit fast diffusion, albeit with a diffusion coefficient that increases with genomic separation. These features give rise to an anomalous scaling of polymer relaxation times and longrange correlations in the relative motion of the two loci. This suggests that the enhancerpromoter search process is much less dependent on genomic separation than expected based on existing polymer models.

Results

Live imaging of chromosome dynamics and transcription

To simultaneously monitor the coupled motion of enhancer-promoter pairs and transcription across multiple genomic separations, we generated fly lines in which a reporter gene was introduced at various genomic locations from the well-studied Drosophila even-skipped (eve) locus (8). The locations of both the endogenous eve enhancers and the promoter of the reporter gene, as well as the transcriptional activity of the reporter gene, were measured together using a three-color imaging system (see the materials and methods, section 1.2, and Fig. 1A) (8). To facilitate transcription, the reporter cassette contained the insulator element homie, which allowed stable loop formation with the endogenous homie element in the eve locus (Fig. 1B).

We built seven such reporter constructs, with genomic separations s varying over close to two orders of magnitude from 58 kb to 3.3 Mb, comparable to the distances over which many enhancers function in higher eukaryotes (see the materials and methods, section 1.1) (9–12). These genomic length scales span across multiple TADs in the *Drosophila* genome, with typical median TAD sizes of ~90 kb (45) (here, 18 kb for the *eve* locus).

Imaging took place for ~30 min during the second half of nuclear cycle 14 (NC14) of

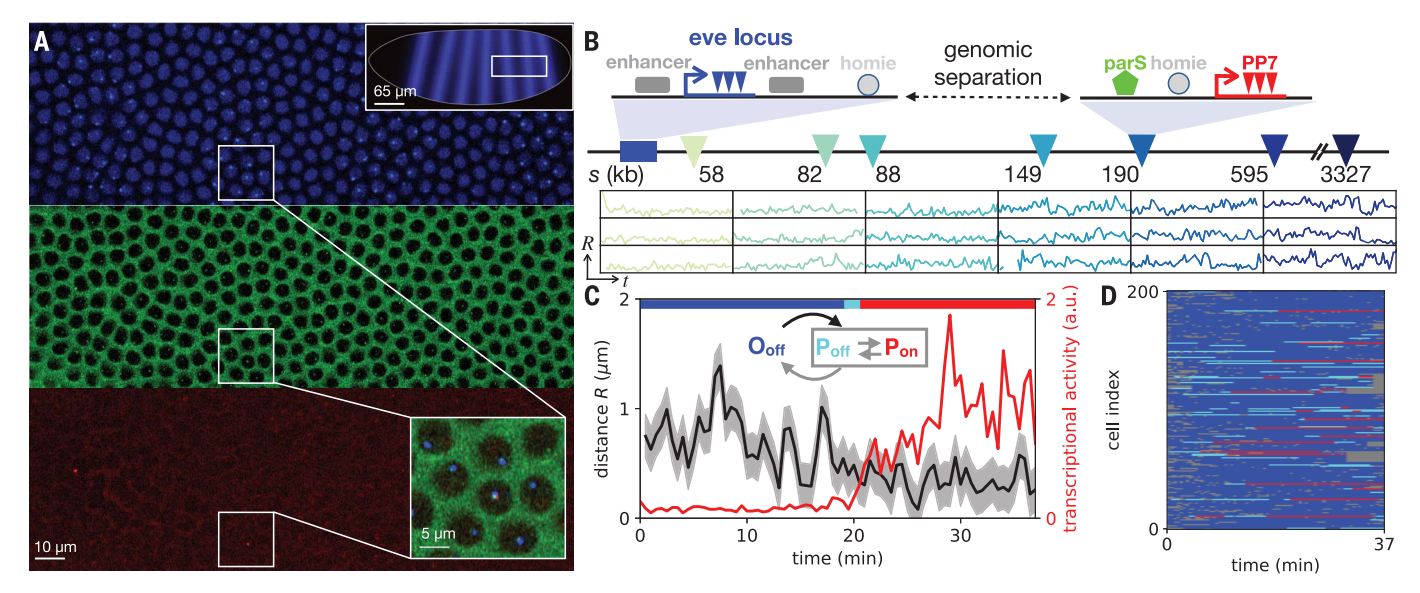


Fig. 1. Simultaneous tracking of DNA loci and transcriptional activity in living embryos. (**A**) Typical surface view of a representative fly embryo displaying fluorescent foci for MS2, parS, and PP7 in the corresponding blue (top), green (center), and red (bottom) channels. Top inset shows schematic with image location in the embryo; bottom inset shows a close-up. (**B**) Top: schematic of the gene cassettes used for three-color imaging. The endogenous eve locus (left) is tagged with MS2 stem loops that are labeled with blue fluorescence. A reporter with an eve promoter driving PP7 transcription (labeled with red fluorescence) is integrated at a genomic separation s from the eve locus on the second chromosome in the *Drosophila* genome. It includes a *homie* insulator sequence allowing loop formation through *homie-homie* pairing and a parS sequence that is permanently labeled with green fluorescence. Seven such

constructs were generated with varying genomic separation s (triangles). Bottom: sample interlocus distance trajectories R(t) for six genomic separations, with standardized y-axis limits (0, 2 μ m) and x-axis limits (0, 30 min) obtained after nucleus and locus segmentation, tracking, chromatic aberration, and motion correction (see the materials and methods, section 1). The sampling time interval is 28 s. (\mathbf{C}) Trajectories of interlocus distance R and transcriptional activity, with inferred topological states shown by the colored top bar (blue, O_{off} ; cyan, P_{off} ; red, P_{on} ; see the materials and methods, section 2). Inset: schematic of the three topological states. (\mathbf{D}) 200 examples of state trajectories sampled from a total set of N = 579 trajectories acquired in n = 30 embryos (genomic separation s = 149 kb). Colors are as in (C). Gray trajectory parts correspond to untrackable time points.

embryo development (Fig. 1C), well after the completion of DNA replication. Sister chromatids are tightly coupled together at intervals <10 kb (46). Therefore, our two tagged DNA loci are connected by a single chromatin polymer composed of two coupled chromatids that were not resolved by our microscopy. Accordingly, our measurements are associated with increased localization uncertainty and reflect both intra- and interchromosomal interactions, which may not be fully representative of pure intrachromosomal interactions.

Interlocus distance scaling suggests a space-filling organization

In previous work using a single fixed genomic distance ($s=149~{\rm kb}$) (s), this system was shown to exhibit three topological states (Fig. 1C): an open configuration, $O_{\rm off}$, in which the homie elements are not bound to each other, and two paired configurations, $P_{\rm off}$ and $P_{\rm on}$, in which a loop is formed with either inactive or active transcription, respectively. Assuming that these configurations apply to all genomic distances, we determined the instantaneous topological and transcriptional states of the system. To this end, we used an

inference approach with a hidden Markov model that is based on the time series of interlocus distances and transcriptional activity (see the materials and methods, section 2). We assigned one of these states to each measured configuration, including the hidden $P_{\rm off}$ state (Fig. 1D).

A key question is how the interlocus distances R in the open configuration O_{off} vary with the linear genomic separation s. These distances exhibit broad distributions, which shift systematically with larger separation (Fig. 2A). From a polymer physics perspective, the mean distance $\langle R \rangle$ is expected to scale as $s^{1/d}$, where d is the fractal dimension. Whereas an ideal chain polymer, as predicted by the simple Rouse model, has fractal dimension d = 2, the compact crumpled chain organization has dimension d = 3 (33, 47). Our experiments show a scaling exponent of 1/d = 0.31 ± 0.07 for genomic separations up to s =190 kb, consistent with the crumpled chain model (Fig. 2B). The smaller-than-expected average distances observed for the largest separations (s = 595 kb, 3.3 Mb) are most likely affected by the average folding of the chromosome (48).

The distances of the paired configurations were independent of genomic separation, as anticipated, and exhibited typical distances of 350 to 400 nm (Fig. 2B), consistent with previous measurements of distances within the *eve* locus (8, 49). Together, these results reveal a compact crumpled chain architecture of chromosome configurations in a range of genomic separations consistent with Hi-C experiments in *Drosophila* (17).

Transcriptional activity scales with genomic separation

From the latent state trajectories revealed by our inference approach, we estimated the survival curves of the transcriptionally active state (see the materials and methods, section 2.4, and Fig. 2C). We found a median transcriptional lifetime independent of genomic separation of 10 \pm 5 min (SD across separations; Fig. 2D). This corresponds to about three to five independent rounds of transcription on average, given the typical promoter switching correlation time of the system (50). Similarly, the relative proportion of transcriptionally active states within the paired subpopulation is insensitive to genomic separation (Fig. 2E).

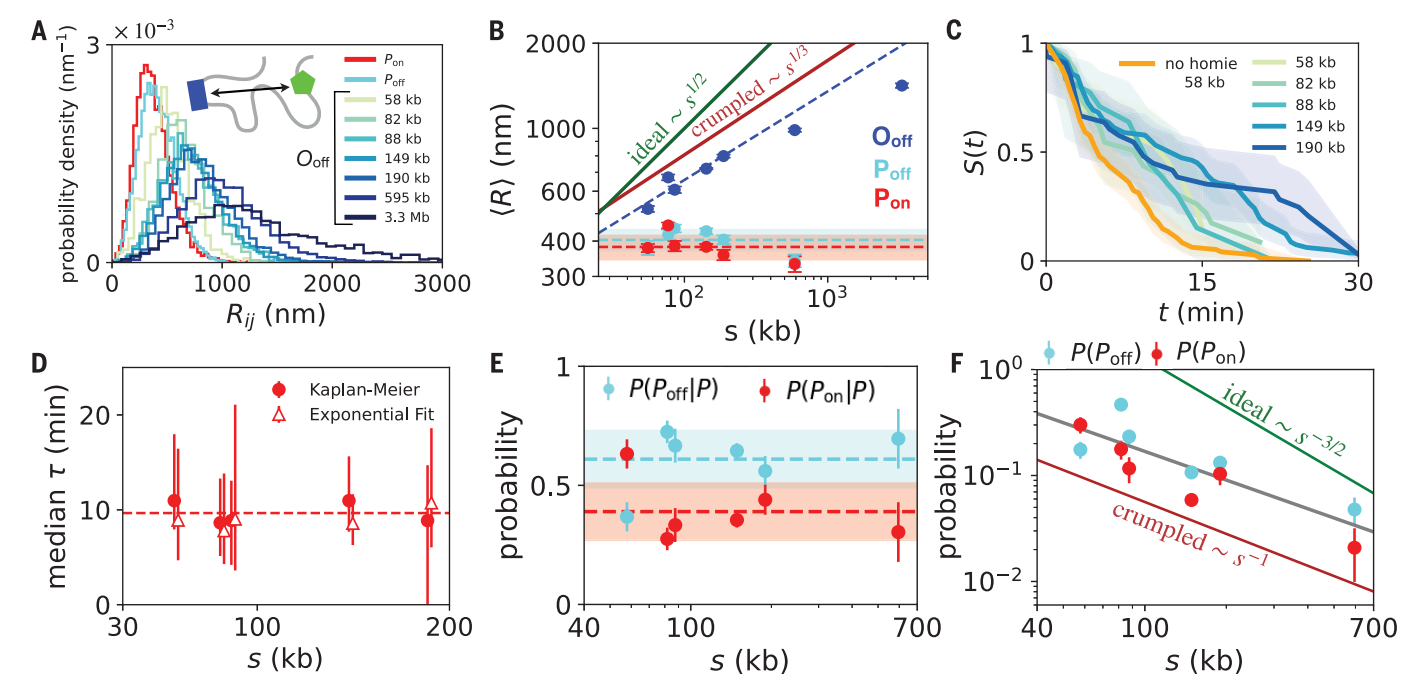


Fig. 2. Scaling of interlocus distances and transcriptional activity across genomic separations. (A) Probability distributions of the interlocus distances R. Distributions are separated by state, with paired states pooled across genomic separations, and individual distributions are shown for the open state. **(B)** Average interlocus distances $\langle R \rangle$ for each of the three transcriptional states. Blue dashed line indicates a linear best fit to the O_{off} data for the range of genomic separations 58 to 190 kb, with exponent $1/d = 0.31 \pm 0.07$. Dashed cyan and red lines are average values of the interlocus distances of the Poff and $P_{\rm on}$ states, respectively, with shaded areas indicating SEM. Solid dark green and red lines indicate predictions for ideal and crumpled polymers, respectively. (C) Survival curves S(t) of the transcriptionally active state P_{on} , giving the probability that transcription remains active after time t. Orange curve: data for no-homie constructs (s = 58 kb). Curves were estimated using the

Kaplan-Meier estimator, which accounts for censoring that occurs if the trajectory begins or ends in the transcriptionally active state (81). Shaded areas show 95% confidence intervals (see the materials and methods, section 2.4). (**D**) Median lifetime of the transcriptionally active state P_{on} as a function of genomic separation using the Kaplan-Meier estimator (dots) and a maximum-likelihood estimator assuming exponential decay of the survival curves (triangles) (see the materials and methods, section 2.4). (E) Probability of the paired on and off states conditioned on the system being in one of these two paired configurations. (F) Overall probability of the paired configurations P_{off} and P_{on} as a function of genomic separation. Gray line is the best fit with exponent 0.9 ± 0.2. Green and dark red lines indicate predicted exponents for the contact probabilities of the ideal and crumpled chain polymer models, respectively.

By contrast, the overall probability of observing either of the paired configurations decreases with genomic separation and exhibits a powerlaw scaling $P(s) \sim s^{-f}$, with $f = 0.9 \pm 0.2$ (Fig. 2F). Because transcriptional lifetimes are independent of distance, the scaling of P(s) is likely dominated by the search of the two loci to come into contact. Different polymer models make distinct predictions of the scaling of contact probabilities (22, 33, 51). For ideal chains, f = 3/2, whereas crumpled chains exhibit $f \approx 1.15$ (52), which is close to the scaling that we observed.

To determine how these results depend on the nature of the homie insulator-mediated focal contacts in our system, we used a reporter construct in which the homie sequence was replaced by a λ DNA sequence of the same length. At a 58-kb separation, transcriptional encounters still occur, albeit with a shorter median lifetime of 4.9 ± 1.2 min (Fig. 2C and fig. S13). Furthermore, the probability of observing a transcriptional state was reduced from

 $(30 \pm 5)\%$ for the *homie* version to $(8.5 \pm 0.8)\%$ in the no-homie version. By contrast, very few such encounters were found for a 149-kb nohomie separation (8), where contact probability decreases from $(6 \pm 1)\%$ to >1% when the *homie* sequence was replaced by a λ DNA.

Together, these results demonstrate quantitatively how both genomic sequence and genomic separation control the rate of transcriptional encounters. The scaling of transcription probabilities with separation suggests that the transition from the open to the paired configuration is a key limiting step in transcriptional activation of distal DNA loci, which is limited by the time taken to diffuse into proximity.

Characterizing the subdiffusive locus search process

To understand these diffusive timescales, we considered the real-time dynamics of the blueand green-labeled DNA loci. We found that the majority of single-cell trajectories sampled the whole range of physical distances in each topological state, because they showed a similar spread as the ensemble-averaged distribution (Fig. 3, A to C, and fig. S8). Thus, rather than existing in constrained configurations as observed in other genomic contexts (41), this observation supports the picture of a dynamic search process exploring a broad range of distances.

We quantified how this search process is reflected in the motion of individual DNA loci by computing the single-locus MSD $M_1(t) =$ $\langle (\mathbf{r}_i(t_0+t)-\mathbf{r}_i(t_0))^2 \rangle_{t_0} = \Gamma t^{\beta}$, where $\mathbf{r}_i(t)$ is the 3D position of the locus, Γ is diffusivity, and β is the dynamic exponent. This exponent quantifies how locus diffusion scales with time and can be related theoretically to the packing of the chromosome through the fractal dimension d: $\beta = 2/(2 + d)$ (37, 39, 53). Although the ideal chain model predicts β = 1/2 (54), we expected $\beta = 2/5$ for a crumpled polymer (37). Our system showed a scaling exponent of $\beta = 0.52 \pm 0.04$ across genomic separations (error bar: SD calculated from

total variance across separations) for both the endogenous eve locus (blue) and the ectopic reporter (green), which is close to the prediction of the ideal chain model and consistent with previous works (26, 27, 35) (see the materials and methods, section 3, and Fig. 3, D and E). Our data further indicate that the singlelocus dynamics are not affected by transcriptional activity, unlike previous accounts (43), because they were consistent across the three topological states (Fig. 3F).

To further understand how the locus dynamics are determined by the interplay of chromosome organization and single-locus dynamics, we analyzed the joint dynamics of the two coupled chromosomal loci. From the statistics of the 3D distance vector $\mathbf{R}(t)$, we computed the twolocus MSD $M_2(t) = \langle (\mathbf{R}(t_0 + t) - \mathbf{R}(t_0))^2 \rangle_{t_0}$ (26), which quantifies the crossover between two intuitive regimes. Whereas at small time lags, the MSD is determined by the independent diffusion of the two loci $[M_2(t) = 2\Gamma t^{\beta}]$, it exhibits a crossover to a plateau at large times, given by the average squared interlocus distance $[M_2(t) = 2\langle R^2 \rangle]$ (see the materials and methods, section 5, and Fig. 4, A and B). Consistent with the observed singlelocus dynamics, we found that the subdiffusive regime of the experimental two-locus MSD exhibited an exponent close to 1/2 for those datasets in which this regime was sampled (Fig. 4A and fig. S16). Similarly, for large time lags, the two-locus autocorrelation revealed agreement with the ideal chain scaling (Fig. 4, C and D). Thus, the full time dependence of the MSD is well described by the ideal chain predictions, both for single and coupled loci.

Interlocus relaxation times exhibit an anomalous scaling with genomic separation

Having established the static and dynamic properties of the system, we next investigated the consequences of these features for the timescales of the two-locus search process. This process is determined by the interplay of chromosome dynamics and organization and can be characterized by a relaxation time τ , which corresponds to the timescale of the crossover of the two regimes of the two-locus MSD (Fig. 2A). Specifically, τ is the time taken by the two loci to diffuse (dynamics) over their typical distance of separation (organization): $\Gamma \tau^{\beta} \sim s^{2/d}$. This relationship predicts a scaling of relaxation times with genomic separation $\tau \sim s^{\gamma}$. For ideal chains with fractal dimension d = 2and a diffusion exponent $\beta = 1/2$, this yields the classical result γ = 2. By contrast, for crumpled chains, $\beta = 2/5$ and d = 3, yielding $\gamma = 5/3$ (see the materials and methods, section 5, and table S7).

To infer the relaxation time in our data as a function of genomic separation, we performed a Bayesian fitting of the two-locus MSD with

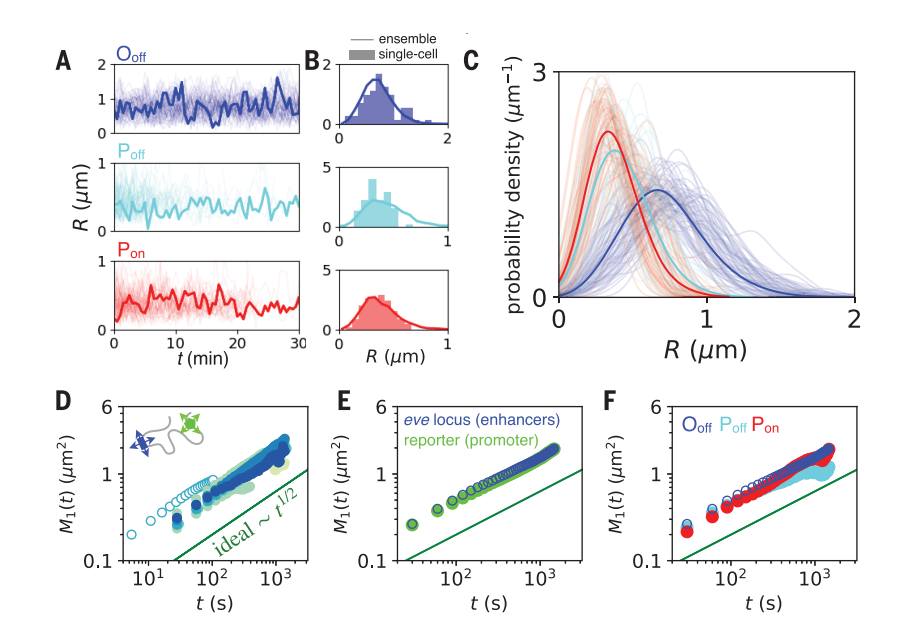


Fig. 3. Dynamics of DNA locus search and single-locus fluctuations. (A) Single-cell interlocus distance trajectories for the three topological states (s = 149 kb). For each state, 80 trajectories are shown, with one sample trajectory highlighted in bold. (B) Distance distributions (bar histogram) of the highlighted trajectory in (C) compared with the ensemble distribution obtained by averaging over all cells (line). (C) Single-cell interlocus distance distributions (thin lines) of all trajectories for the three states compared with ensemble distributions in bold (s = 149 kb). Distributions are smoothed using Gaussian kernel density estimation with a width of 100 nm. Only trajectories with at least 10 time points are included to ensure sufficient statistics for comparison. (D) Single-locus MSDs for all genomic separations (color code corresponds to Fig. 2A). Single-locus MSDs were calculated by estimating 3D MSDs from motion-corrected trajectories in the x-y plane of the system (see the materials and methods, section 3). Open data points correspond to a shorter imaging time interval $\Delta t = 5.4$ s (s = 149 kb). (E) Single-locus MSDs comparing enhancer (blue) and promoter (green) fluctuations (s = 149 kb).

(**F**) Single-locus MSDs comparing fluctuations in the three states (s = 149 kb).

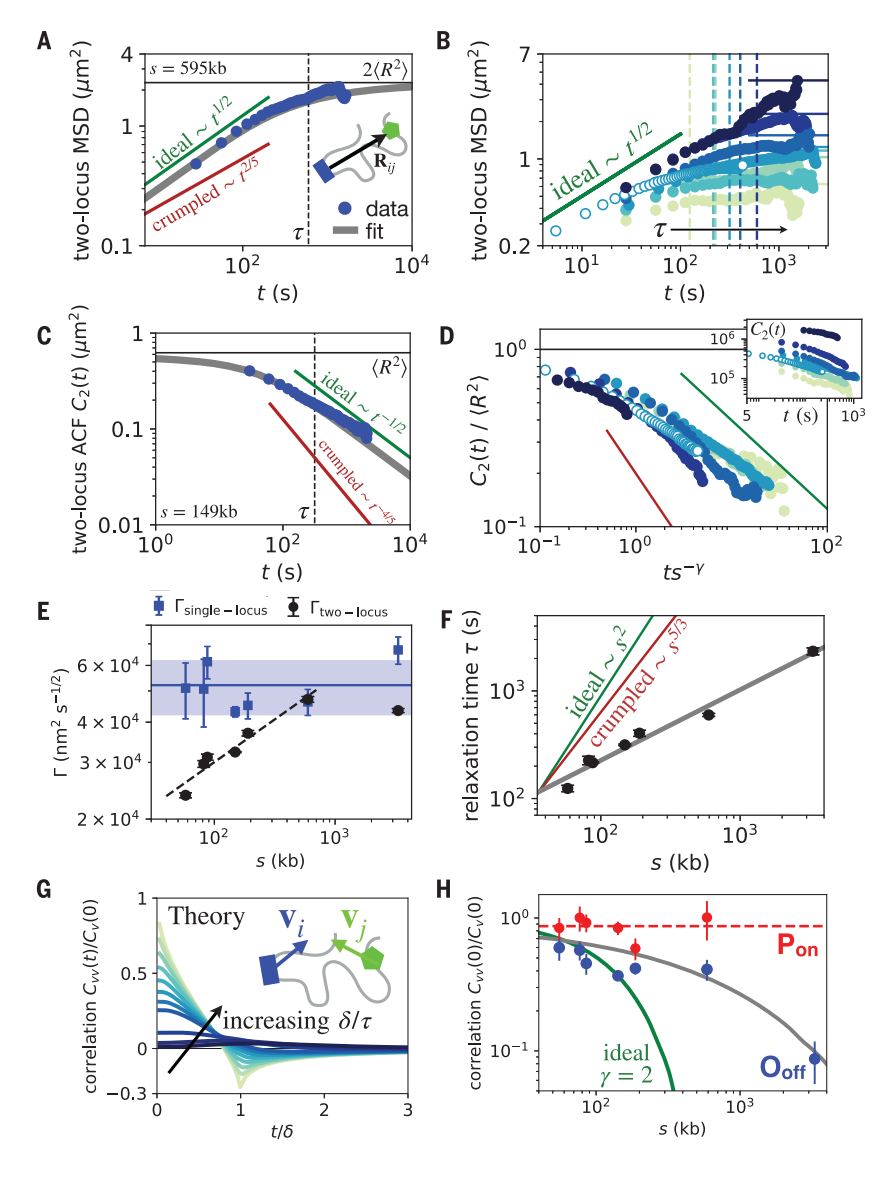
the ideal chain expression (26) (see the materials and methods, section 4.1). We found that the fitted two-locus diffusion coefficient increased with genomic separation up to 595 kb, with an approximate scaling $\Gamma(s) \sim s^{0.27 \pm 0.03}$ (Fig. 4E). This scaling appeared to plateau for the largest genomic separation (3.3 Mb) at a value close to the single-locus diffusion, which remained approximately constant across separations (Fig. 4E). The absolute value of the diffusivity at the plateau was almost 20-fold larger than previous measurements in mammalian stem cells with similar genomic separation (26), suggesting comparatively fast chromosome dynamics (fig. S23).

The relaxation time was determined by combining our estimate of the two-locus diffusivity with the average interlocus distances. The combination of static and dynamic exponents in our system, as well as the scale-dependent diffusivity, results in an anomalous scaling of relaxation times with genomic separation with an exponent $\gamma = 0.7 \pm 0.2$ (Fig. 4F). This exponent corresponds to a much shallower scaling with separation than predicted by either the ideal or crumpled chain theory. This result was further confirmed by a data collapse of the two-locus autocorrelation functions (Fig. 4D and fig. S20). Although these results are derived from the trajectories in the O_{off} state, they are insensitive to the details of the state inference (fig. S11). In sum, the key result here is that the relaxation time, which sets the timescale of two-locus encounters, is much less dependent on genomic separation than predicted by existing polymer models.

Anomalous relaxation time scaling induces long-ranged velocity correlations

The anomalous relaxation time scaling makes a key prediction for the correlations of the absolute motion of DNA loci, quantified by the velocity cross-correlation $C_{vv}^{(\delta)}(t) = \langle \mathbf{v}_i^{(\delta)}(t_0) \rangle$ $\mathbf{v}_{i}^{(\delta)}(t_{0}+t)\rangle_{t_{0}}$. These correlations are determined by the relaxation time through the dimensionless ratio δ/τ , where δ is the experimental observation timescale (Fig. 4G) (55). Having determined the relaxation times τ , one can therefore make a parameter-free prediction of the correlations, which decay

Fig. 4. Joint dynamics of DNA locus pairs. (A) Ideal chain Rouse prediction of the two-locus MSD $M_2(t)$ = $2\Gamma t^{1/2}(1 - e^{-\tau/\pi t}) + 2J \operatorname{erfc}[(\tau/\pi t)^{1/2}]$ (26) (gray line) using best-fit values Γ , J, β = 1/2, and τ = $(J/\Gamma)^2$, compared with experiment (s = 595 kb). Green and red lines give expected scaling t^{β} for $t \ll \tau$ for the generalized Rouse model for ideal and crumpled chains, respectively (see the materials and methods, section 5). (B) All experimental two-locus MSDs with relaxation times (dashed lines) and expected asymptotes $2\langle R^2\rangle$ (solid lines; color code corresponds to Fig. 2A). (**C**) Scaling of the diffusion coefficients Γ from two-locus MSD fits (black dots) compared with single-locus diffusion coefficients obtained from single-locus MSDs (Fig. 3, F to H). Dashed line is the best fit to two-locus diffusivity with exponent 0.27 ± 0.03 (s = 58 to 595 kb); solid lines are the average value of singlelocus diffusivities; shaded area shows SE calculated from total variance across separations. (D) Two-locus autocorrelation function (ACF) $C_2(t) = \langle R(t_0) \cdot R(t_0 + t) \rangle_{t_0} =$ $\langle R^2 \rangle - M_2(t)/2$ (gray) compared with data (s = 149 kb). Green and red curves indicate the power-law exponent $\lambda = 2(1-d)/(2+d)$ of the correlation function $C_2(t) \sim t^{\lambda}$ for ideal and crumpled chains for $t \gg \tau$, respectively (39). (**E**) Collapsed correlations $C_2 \sim C_2(ts^{-\gamma})/\langle R^2 \rangle$ with γ = 0.7. Inset: raw correlations $C_2(t)$ for varying genomic separation. Open data points correspond to data obtained with a higher sampling rate. (F) Scaling of inferred relaxation times compared with predicted ideal and crumpled chain exponents. Gray line is the best fit with exponent γ = 0.7 ± 0.2. (**G**) Predicted velocity cross-correlation functions $C_{vv}^{(\delta)}(t) =$ $\langle v_i^{(\delta)}(t_0)\cdot v_j^{(\delta)}(t_0+t)\rangle_{t_0}$ for increasing values of the dimensionless ratio δ/τ (55). Velocities are calculated on a time interval δ as $\mathbf{v}^{(\delta)}(t) = [\mathbf{x}(t+\delta) - \mathbf{x}(t)]/\delta$. (H) Scaling of the zero-time velocity cross-correlation intercept normalized by the zero-time autocorrelation, $C_{vv}^{(\delta)}(0)/C_{v}^{(\delta)}(0)$, for the O_{off} (blue) and P_{on} (red) states; δ = 300 s. Green line is the prediction based on ideal chain Rouse scaling of the relaxation times ($\gamma = 2$) with an intercept determined based on the 58-kb data point; grav



line is the parameter-free prediction using the inferred anomalous relaxation time scaling ($\gamma \approx 0.7$) (see the materials and methods, section 4.3); dashed red line is the average correlation in the P_{on} state.

substantially more slowly than for the ideal Rouse model (see the materials and methods, section 4.3, and Fig. 4H, green and gray lines). We found that the experimental correlations were quantitatively captured by this parameter-free prediction (Fig. 4H), including the full time dependence of the correlations (fig. S22). This demonstrates that the anomalous relaxation time scaling indeed leads to long-range velocity cross-correlations of chromosomal loci, pointing toward potential long-range interactions.

Discussion

We developed an experimental approach to perform in vivo imaging of the joint dynamics of enhancer-promoter pairs with varying genomic separation and simultaneous monitoring of their transcriptional output. Observing the dynamics of pairs of DNA loci has only become possible recently and has been done for tagged DNA loci at a single fixed genomic separation (8, 26, 27, 36). Here, we show how imaging across genomic separations gives insight into the relative motion, dynamic encounters, and transcriptional activation of such loci.

Many features of the two-locus dynamics, including the subdiffusive exponent close to 0.5, are very well conserved with measurements of CTCF sites at TAD boundaries in mammalian systems (26, 27), despite CTCF not being essential for *Drosophila* embryogenesis (56). In absolute numbers, however,

our measurements revealed large diffusion coefficients of DNA loci that are ~20-fold larger than in mammalian cells (26) (fig. S23). Early fly development follows a tight schedule, suggesting that the chromosome dynamics may have evolved to operate on much faster timescales than mammalian systems. By contrast, the median lifetime of focal contacts in our system of 12 ± 5 min is well within the range of typical CTCF loop lifetimes of 10 to 30 min in mammalian cells (26, 27). These timescales facilitate transcriptional lifetimes of 10 ± 5 min in our system, which in the absence of the homie insulator are reduced to 4.9 ± 1.2 min (Fig. 2C and fig. S13), highlighting the importance of focal elements for contact formation in Drosophila.

times and were ~10 times larger on average

(fig. S19).

We have demonstrated how key features of our system, tight crumpled chain packing, subdiffusion with exponent 0.5, and a separationdependent two-locus diffusivity, lead to relaxation times that are much less dependent on genomic separation than predicted by existing polymer models. Indeed, for an ideal Rouse polymer, the relaxation time for our largest genomic separation (3.3 Mb) would be ~3000 times longer than for the shortest 58-kb separation. Our measurements, however, revealed that it only takes ~20 times longer, corresponding to a >100-fold reduction. This reduced dependence on distance implies that transcriptional encounters are possible across large genomic distances, allowing enhancers dispersed across the chromosome to find their target promoter efficiently. This might be one of the reasons that evolution can act on distal sequences from a given target promoter. Overall, our findings have crucial implications for the spatiotemporal organization of the cell nucleus. including the dynamics of long-range focal contacts (28) and mammalian enhancer-promoter interactions (9-12, 44).

From a polymer physics perspective, our measured exponents suggest that the relationship between static and dynamic properties in the generalized Rouse framework, which relies on the assumption of local friction, does not apply to chromosomes. This implies that long-range interactions such as hydrodynamics or active motor-mediated interactions (60, 61) could play a role. Indeed, the simplest polymer model that relaxes the Rouse assumption and includes long-range hydrodynamic interactions, the Zimm model (54), predicts a scaling relationship of relaxation times with genomic separations with an exponent of $\gamma = 1$ (table S7), which is close to our measured value of $\gamma \approx 0.7$. Furthermore, the observed separation-dependent diffusivity points to additional interactions or heterogeneities along the polymer. Such heterogeneities could be caused by a number of processes, such as cross-linking (41), out-of-equilibrium activity (61), entanglements (62), or the presence of condensates (18-20). Together, these processes may orchestrate the anomalous scaling of relaxation times with genomic sep-

aration. In future work, the mechanistic underpinnings of our findings should be tested using polymer simulations (40, 41, 51, 63-69) to generate hypotheses for new sets of experiments.

REFERENCES AND NOTES

- 1. W. Flemming. Zellsubstanz, Kern Und Zelltheilung (Vogel, 1882)
- 2. R. Milo, R. Phillips, Cell Biology by the Numbers (CRC Press,
- R. Stadhouders, G. J. Filion, T. Graf, Nature 569, 345-354 (2019)
- B. van Steensel, E. E. M. Furlong, Nat. Rev. Mol. Cell Biol. 20, 327-337 (2019)
- 5. M. Levine, Curr. Biol. 20, R754-R763 (2010).
- T. K. Kim, R. Shiekhattar, Cell 162, 948-959 (2015).
- D. Vernimmen, W. A. Bickmore, Trends Genet. 31, 696-708 (2015).
- H. Chen et al., Nat. Genet. 50, 1296-1303 (2018).
- B. Tolhuis, R. J. Palstra, E. Splinter, F. Grosveld, W. de Laat, Mol. Cell 10, 1453-1465 (2002).
- 10 V V Uslu et al. Nat. Genet. 46, 753-758 (2014).
- 11. Y. Zhang et al., Nature 504, 306-310 (2013).
- 12. A. Sanyal, B. R. Lajoie, G. Jain, J. Dekker, Nature 489, 109-113 (2012)
- 13. Y. Huang, R. Neijts, W. de Laat, FEBS Lett. 594, 3439-3449 (2020).
- 14. J. R. Dixon et al., Nature 485, 376-380 (2012).
- 15. C. Hou, L. Li, Z. S. Qin, V. G. Corces, Mol. Cell 48, 471-484 (2012)
- 16. E. P. Nora et al., Nature 485, 381-385 (2012).
- 17. T. Sexton et al., Cell 148, 458-472 (2012).
- 18. A. Boija et al., Cell 175, 1842-1855.e16 (2018).
- 19. W.-K. Cho et al., Science 361, 412-415 (2018).
- 20. M. Conte et al., Nat. Commun. 13, 4070 (2022)
- 21. C. S. Osborne et al., Nat. Genet. 36, 1065-1071
- 22. E. Lieberman-Aiden et al., Science 326, 289-293 (2009).
- 23. O. Symmons et al., Genome Res. 24, 390-400 (2014).
- 24. T. J. Stevens et al., Nature 544, 59-64 (2017).
- 25. M. V. Arrastia et al., Nat. Biotechnol. 40, 64-73 (2022).
- 26. M. Gabriele et al., Science 376, 496-501 (2022).
- 27. P. Mach et al., Nat. Genet. 54, 1907-1918 (2022).
- 28. M. Levo et al., Nature 605, 754-760 (2022).
- 29. S. Wang et al., Science 353, 598-602 (2016).
- 30. B. Bintu et al., Science 362, eaau1783 (2018).
- 31. A. Grosberg, Y. Rabin, S. Havlin, A. Neer, Europhys. Lett. 23, 373-378 (1993).
- 32. A. Yu. Grosberg, S. K. Nechaev, E. I. Shakhnovich, J. Phys. (Paris) 49, 2095-2100 (1988).
- 33. L. A. Mirny, Chromosome Res. 19, 37-51 (2011).
- 34. S. C. Weber, A. J. Spakowitz, J. A. Theriot, Phys. Rev. Lett. 104, 238102 (2010).
- 35. J. S. Lucas, Y. Zhang, O. K. Dudko, C. Murre, Cell 158, 339-352 (2014)
- 36. J. M. Alexander et al., eLife 8, e41769 (2019).
- 37. M. V. Tamm, L. I. Nazarov, A. A. Gavrilov, A. V. Chertovich, Phys. Rev. Lett. 114, 178102 (2015).
- 38. S. Shinkai, T. Nozaki, K. Maeshima, Y. Togashi, PLOS Comput. Biol. 12, e1005136 (2016).
- 39. K. E. Polovnikov, M. Gherardi, M. Cosentino-Lagomarsino, M. V. Tamm, Phys. Rev. Lett. 120, 088101 (2018).
- 40. M. Nicodemi, A. Pombo, Curr. Opin. Cell Biol. 28, 90-95 41. N. Khanna, Y. Zhang, J. S. Lucas, O. K. Dudko, C. Murre,
- Nat. Commun. 10, 2771 (2019).
- 42. T. Germier et al., Biophys. J. 113, 1383-1394 (2017).
- 43. B. Gu et al., Science 359, 1050-1055 (2018).
- 44. J. Zuin et al., Nature 604, 571-577 (2022). 45. S. V. Ulianov et al., Nat. Commun. 12, 41 (2021).
- 46. B. L. Hua, T. L. Orr-Weaver, Genetics 207, 29-47 (2017).
- 47. B. Avşaroğlu et al., PLOS ONE 9, e102474 (2014).
- 48. J. Dekker, M. A. Marti-Renom, L. A. Mirny, Nat. Rev. Genet. 14, 390-403 (2013).
- 49. L. Barinov, S. Ryabichko, W. Bialek, T. Gregor, Transcriptiondependent spatial organization of a gene locus. arXiv:2012. 15819 [q-bio.MN] (2020).

- 50. B. Zoller, S. C. Little, T. Gregor, Cell 175, 835-847.e25 (2018)
- 51 A Rosa N B Becker R Everaers Biophys J 98 2410-2419 (2010).
- 52. J. D. Halverson, W. B. Lee, G. S. Grest, A. Y. Grosberg, K. Kremer, J. Chem. Phys. 134, 204904 (2011).
- 53. P. G. De Gennes, Macromolecules 9, 587-593 (1976).
- 54. M. Rubinstein, R. H. Colby, Polymer Physics (Oxford Univ. Press 2003)
- 55. T. J. Lampo, A. S. Kennard, A. J. Spakowitz, Biophys. J. 110, 338-347 (2016).
- . A. Kaushal et al., Nat. Commun. 12, 1011 (2021)
- 57. G. Wilemski, M. Fixman, J. Chem. Phys. 60, 866-877 (1974).
- 58. A. Szabo, K. Schulten, Z. Schulten, J. Chem. Phys. 72, 4350-4357 (1980).
- 59. M. Fujioka, H. Mistry, P. Schedl, J. B. Jaynes, PLOS Genet. 12, e1005889 (2016).
- 60. R. Bruinsma, A. Y. Grosberg, Y. Rabin, A. Zidovska, Biophys. J. 106, 1871-1881 (2014).
- 61. M. M. Tortora, H. Salari, D. Jost, Curr. Opin. Genet. Dev. 61, 37-43 (2020).
- 62. R. Kawamura et al., J. Cell Biol. 188, 653-663 (2010).
- 63. A. Rosa, R. Everaers, PLOS Comput. Biol. 4, e1000153
- 64. M. Barbieri et al., Proc. Natl. Acad. Sci. U.S.A. 109, 16173-16178 (2012).
- 65. L. Giorgetti et al., Cell 157, 950-963 (2014).
- 66. L. Liu, G. Shi, D. Thirumalai, C. Hyeon, PLOS Comput. Biol. 14, e1006617 (2018).
- 67. A. Buckle, C. A. Brackley, S. Boyle, D. Marenduzzo, N. Gilbert, Mol. Cell 72, 786-797.e11 (2018).
- 68. C. A. Brackey, D. Marenduzzo, N. Gilbert, Nat. Methods 17, 767-775 (2020).
- 69. H. Salari, M. Di Stefano, D. Jost, Genome Res. 32, 28-43 (2022)
- 70. D. B. Brückner, B. Zoller, dbrueckner/DynamicChromosome: initial release, Zenodo (2023); https://zenodo.org/record/
- 71. D. B. Brückner, H. Chen, L. Barinov, B. Zoller, T. Gregor, Trajectory data for: Stochastic motion and transcriptional dynamics of pairs of distal DNA loci on a compacted chromosome, Zenodo (2023); https://zenodo.org/record/ 7616203

ACKNOWLEDGMENTS

We thank R. Evearers, L. Giorgetti, A. Grosberg, S. Grosse-Holz, M. Levo, L. Mirny, A. Rosa, V. Scolari, A. Spakowitz, and G. Tkacik for helpful comments and discussion; K. Bystricky for introducing us to the ParB/parS system; and F. Payre and P. Valenti for sharing the ParB-eGFP plasmid and the parS sequence. Funding: This work was supported in part by the U.S. National Science Foundation, the Center for the Physics of Biological Function (grant PHY-1734030), and the National Institutes of Health (grants R01GM097275, U01DA047730, and U01DK127429). D.B.B. was supported by the NOMIS Foundation as a fellow and by an EMBO postdoctoral fellowship (ALTF 343-2022). H.C. was supported by a Charles H. Revson Biomedical Science Fellowship. Author contributions: H.C. and T.G. designed the experiments. H.C. and L.B. performed the experiments and analyzed the images. D.B.B. and B.Z. analyzed the data, D.B.B. and T.G. interpreted the data, D.B.B., B.Z., and T.G. wrote the manuscript, Competing interests: The authors declare no competing interests. Data and materials availability: The code and software used in this study (70) and the raw trajectory data (71) are freely available through Zenodo. License information: Copyright © 2023 the authors, some rights reserved; exclusive licensee American. Association for the Advancement of Science. No claim to original US government works. https://www.science.org/about/sciencelicenses-iournal-article-reuse

SUPPLEMENTARY MATERIALS

science.org/doi/10.1126/science.adf5568 Materials and Methods

Figs. S1 to S23 Tables S1 to S8

References (72-86) Movies S1 to S7

MDAR Reproducibility Checklist

View/request a protocol for this paper from Bio-protocol.

Submitted 29 October 2022; accepted 31 May 2023 10.1126/science.adf5568



Stochastic motion and transcriptional dynamics of pairs of distal DNA loci on a compacted chromosome

David B. Brckner, Hongtao Chen, Lev Barinov, Benjamin Zoller, and Thomas Gregor

Science, 380 (6652), .

DOI: 10.1126/science.adf5568

Editor's summary

A crucial step in gene regulation is the physical encounter of dispersed enhancer-promoter pairs across the genome. However, how distal DNA elements find each other in the nuclear space remains unclear. Brückner *et al.* visualized the three-dimensional motion of pairs of DNA loci of varying separations along the chromosome and their transcriptional output in developing fly embryos. They found an unexpected combination of dense packing and rapid diffusion, leading to encounter times with a weak dependence on genomic separation. These results imply that transcriptional contacts are possible across large genomic distances, with crucial implications for gene regulation. —Di Jiang

View the article online

https://www.science.org/doi/10.1126/science.adf5568

Permissions

https://www.science.org/help/reprints-and-permissions

Use of this article is subject to the Terms of service